Article:
Alcott, LJ, Mills, BJW and Poulton, SW (2019) Stepwise Earth oxygenation is an inherent property of global biogeochemical cycling. Science, 366 (6471). pp. 1333-1337. ISSN: 0036-8075

https://doi.org/10.1126/science.aax6459

Title: Stepwise Earth oxygenation is an inherent property of global biogeochemical cycling

Authors: Lewis J. Alcott[1]*, Benjamin J. W. Mills[1], Simon W. Poulton[1]

Affiliations: [1]School of Earth and Environment, University of Leeds, Leeds LS2 9JT, UK.

*Correspondence to: eelja@leeds.ac.uk

Abstract: Oxygenation of Earth's atmosphere and oceans occurred across three major steps during the Paleoproterozoic, Neoproterozoic, and Paleozoic Eras, with each increase having profound consequences for the biosphere. Biological or tectonic revolutions have been proposed to explain each of these stepwise increases in oxygen, but the principal driver of each event remains unclear. Here we show, using a theoretical model, that the observed oxygenation steps are a simple consequence of internal feedbacks within the long term biogeochemical cycles of carbon, oxygen and phosphorus, and there is no requirement for a specific 'stepwise' external forcing to explain the course of Earth surface oxygenation. We conclude that Earth's oxygenation events are entirely consistent with gradual oxygenation of the planetary surface following the evolution of oxygenic photosynthesis.

One Sentence Summary: Earth's 'stepwise' oxygenation events were driven by internal feedbacks and are consistent with a gradual shift in surface redox state.

Main Text:

Oxygenation of Earth's surface environment is thought to have occurred across three broad steps (Fig. 1). The 'Great Oxidation Event' (GOE) occurred around 2.4 - 2.2 billion years ago (Ga) and saw atmospheric oxygen rise from trace levels to greater than 10^{-5} PAL (Present Atmospheric Level) (*1*). The following ~1 billion years of the Proterozoic Eon likely sustained atmospheric oxygen levels of ~10^{-3} – 10^{-1} PAL (*2*). Partial oxygenation of the surface ocean persisted throughout the Proterozoic (*3*), but deeper waters remained dominantly anoxic (*4*). The 'Neoproterozoic Oxygenation Event' (NOE) occurred between ~800 and 540 Ma, and is generally believed to have resulted in atmospheric oxygen levels of 0.1 - 0.5 PAL, as well as the first oxygenation of the deep ocean (*5*). However, there was considerable variability in the temporal and spatial extent of deep ocean oxygenation at this time, including the possibility of pulsed 'Oceanic Oxic Events' (*6*). Evidence for periodic deep water anoxia remains frequent up until the mid-Paleozoic, when a final major rise in atmospheric oxygen concentration occurred around 450 to 400 Ma (*7*). This 'Paleozoic Oxygenation Event' (POE) appears to have elevated atmospheric O_2 to present day levels, and established a dominantly oxygenated deep ocean, which persisted throughout the Mesozoic and Cenozoic Eras.

These major oxygenation steps are intertwined with the evolution of progressively more complex lifeforms. The first eukaryotes evolved either following the GOE, or during the run-up to the event when O_2 began to rise (*8*), while the NOE is coincident with major eukaryote diversification and the evolution of the first animals (*9*), followed by the 'Cambrian Explosion' where animals began to dominate marine ecosystems. The POE is accompanied by a major increase in animal body size, more diverse and specialized predators, and the evolution of vascular land plants (*7*). However, determining causality between rises in marine and atmospheric O_2 levels and the evolution of the biosphere is complex, and there is considerable

debate over the role of oxygen in driving biological evolution versus the role of life in 'bioengineering' oxygen to higher levels (*10, 11*).

Tectonic evolution has also been considered a potential driver of the stepwise transitions in Earth surface oxygenation. Changes to plate tectonics have been linked to the GOE through, for example, a change in the fraction of subaerial volcanism (*12*) or the composition of the crust (*13*). Some, but not all, supercontinent formation times correspond to oxygenation events (*14*), as do emplacement times of some Large Igneous Provinces (LIPs), which are proposed to have driven ocean oxygenation through delivery of the limiting nutrient, phosphate (*15*).

However, the geologically-rapid yet ultimately rare nature of Earth's oxygenation events does not clearly correspond to either tectonic or evolutionary processes. For example, mantle dynamics and the supercontinent cycle are unlikely to produce large-scale changes on timescales of the order of less than ~100 Myr, whilst LIP emplacements are far more common than major rises in O_2. Looking to biological innovations, the timescale between the origination of a domain or kingdom of life and its rise to global ecological dominance may also be 100's of Myrs (e.g. Eukarya (*16*)). Furthermore, the oscillations in ocean redox apparent during the NOE are difficult to explain via a sequence of tectonic or biological 'switches' acting on the system (e.g.(*17*)).

It is therefore possible that Earth's stepwise oxygenation was not the product of individual trigger events and may instead be explained by some inherent property of global biogeochemical feedbacks. This hypothesis has wide implications for the evolution of life on Earth and other planets, and there have therefore been a number of attempts to explain the known 'stepwise' oxygen trajectory as a feature of Earth's internal dynamics: for example, it has been shown that atmospheric feedbacks might promote the GOE (*18, 19*). However, no study has provided a sound theoretical basis that can explain the trajectory and timings of

marine and atmospheric oxygenation over Earth history without relying either on external 'trigger events' or on arbitrary switches within the model itself (such as assuming a transition to greater nutrient availability when O_2 crosses a threshold (*20, 21*)).

Here we identify a set of feedbacks that exist between the global phosphorus, carbon and oxygen cycles, which are capable of driving rapid shifts in ocean and atmospheric O_2 levels without requiring any 'stepwise' change in either tectonics or the evolution of the biosphere. These feedbacks reproduce the observed 3-step oxygenation pattern when driven solely by a gradual shift from reducing to oxidizing surface conditions over time.

Phosphorus (P) is generally considered the ultimate limiting nutrient for marine productivity over geological timescales (*22*), and P bioavailability exerts a key control on the long-term rate of O_2 production through oxygenic photosynthesis and organic carbon burial. In the modern ocean, bioavailable phosphorus is fixed in the sediments via three primary pathways. Organic-bound P (P_{org}) is buried with sinking organic matter, iron-bound P (P_{Fe}) forms as P is adsorbed or co-precipitated with iron (oxyhydr)oxide minerals, and authigenic P (P_{auth}) is primarily formed within the sediment via 'sink switching' of these phases to carbonate fluorapatite and/or vivianite (*23-25*).

The phase partitioning of sedimentary phosphorus is largely controlled by redox conditions in the water column and sediments. Phosphorus may be preferentially released from organic matter during remineralization under anoxic conditions, leading to elevated C_{org}:P_{org} ratios within the sediment (*26*), increased recycling of P back to the water column, and reduced formation of authigenic carbonate fluorapatite (*27, 28*). The availability of iron (oxyhydr)oxides is also typically considered to diminish in an anoxic system which limits burial of P_{Fe} (*23*), although this dynamic becomes more complex when considering the prevalence of low sulphate, ferruginous (anoxic Fe-rich) oceanic conditions throughout large

parts of Earth history (*4*), whereby Fe minerals may trap a proportion of the P delivered to the sediment (*29*).

Assuming that bottom-water anoxia leads to an overall enhancement of sedimentary P regeneration, two important feedback mechanisms arise that affect global biogeochemistry, with each operating over a different timescale. Firstly, a 'short-term' positive feedback mechanism (self-promoting) operates, whereby the spread of ocean anoxia results in increased phosphorus availability in the water column. This stimulates primary productivity and fuels respiration, thus further increasing phosphorus availability (*26*). These eutrophic conditions rapidly deplete water column oxygen and in turn increase the rate of spread of anoxia. Secondly, a geologically-paced negative feedback mechanism (self-inhibiting) operates on the combined C-O-P cycles, whereby the burial of organic carbon in marine sediments leads to oxygenation of the atmosphere. This increase in pO_2 drives higher rates of oxidative weathering of ancient sedimentary organic C (*30*), and ventilates the ocean, acting to stabilize O_2 both by reducing the rate of organic carbon burial and by increasing the consumption of oxygen on land.

Theoretical models have previously linked the above feedbacks to the geologically-rapid onset of Cretaceous Ocean Anoxic Events (OAEs), and to their delayed termination via increasing atmospheric O_2 (*28*). It has also been shown that under an increased continental weathering input of phosphorus, self-sustaining oscillations between oxic and anoxic oceanic states might occur (*31*). We hypothesize here that the above feedbacks are in fact sufficient to explain the stepwise oxygenation of Earth's atmosphere and oceans, including apparent cyclic ocean oxygenation/deoxygenation events during the Neoproterozoic and early Phanerozoic (*6*), which are followed by the transition to a sustained oxic deep ocean.

Firstly, the GOE can occur when the weathering of organic carbon becomes the principal long-term oxygen sink. This can be achieved once the rate of photosynthetic oxygen

production outpaces the consumption of oxygen via reaction with reduced gases and reduced seawater species. Secondly, cyclic oxygenation events in the NOE would be a likely consequence of the combined positive and negative feedbacks between ocean oxygenation and sedimentary P recycling, whereby a small shift towards a more oxygenated planetary surface results in gradual oxygenation of oceanic bottom waters. This would limit P regeneration from sediments, reducing short-term productivity and oxygen demand, and thus further increasing dissolved oxygen concentrations. This positive feedback could oxygenate ocean basins, but only temporarily, as reduced P availability for primary productivity then leads to less O_2 production over geologic timescales, thus reducing atmospheric O_2, which eventually leads to a return to marine anoxia. Finally, a combination of the two mechanisms outlined above can result in sustained oceanic oxygenation. In this case, a sufficiently large increase in surface redox potential, coupled with a greater contribution of oxidative weathering to overall O_2 regulation, allows deep ocean oxygenation to be maintained.

We test our hypothesis by building upon a well-established conceptual model of marine biogeochemistry (*28, 32, 33*). The model tracks the global cycles of phosphorus, carbon and oxygen within a 4-box ocean system representing shelf, open-ocean and deep water environments (Fig. 2). We add to the model an atmospheric oxygen reservoir, a global geological oxygen cycle, oxidative weathering of organic carbon, and an open-ocean scavenging flux of P by upwelled Fe, basing these on other previous models (*29, 30*).

Phosphorus-dependent primary productivity occurs in all surface ocean boxes, and redox-dependent burial of P is included in all boxes in contact with the sediments. As in previous versions of the model, sedimentary inventories are not calculated explicitly, and regeneration of P from sediments is addressed via the net P burial terms, which follow previous model derivations (*28, 32*). Deep ocean dissolved oxygen concentration is calculated explicitly, as is the oxygen content of the atmosphere. Following previous model versions, the oxygen

content of the ocean boxes in contact with the atmosphere is represented by a 'degree of anoxia' parameter, which we term f_{anoxic} and which represents the balance between O_2 diffusion from the atmosphere and oxygen utilization (*32*). An optional scavenging flux of phosphorus sorption to upwelling iron particles (*29*) is implemented in order to test the effects of additional phosphorus draw-down in a ferruginous (iron-rich) ocean – a state which may have persisted throughout much of Earth history (*4*). The scavenging flux directly follows previous models (*29*), operating at oxygen concentrations below 1 μM and removing 25% of P that is upwelled into the open ocean. Full model equations are shown in the Supplementary Information. As well as testing different limits on the scavenging flux, we also ran sensitivity tests to vary the degree of redox dependency of the P_{org} and P_{auth} burial terms (following previous versions of this model).

Figure 3 shows steady state responses of the baseline model to variable fluxes of reduced gas to the surface system, representing overall changes in net surface redox over Earth history. All other parameters remain at their present day values, and processes vary only via internal feedbacks. The redox dependence of the P_{org} and P_{auth} burial fluxes were varied and are shown as different lines. The model runs with stronger redox dependencies (40% for P_{auth}, 25% for P_{org}) responded first to oxygenation (left-most lines in Fig. 3), and weaker dependencies (35% for P_{auth}, 25% for P_{org} and 10% for both P_{auth} and P_{org}) plot to the right of these. Under a very high reductant flux (left side of x-axis in Fig. 3), as proposed for the Archean ($>>1 \times 10^{13}$ mol O_2 equivalent reductant input (*34, 35*)), O_2 production is overwhelmed and atmospheric O_2 is stable at around 10^{-5} PAL, consistent with pre-GOE conditions (*36*). Here, the O_2 balance is primarily maintained by reaction of O_2 with reduced gases (*30*). All surface and deep ocean boxes are anoxic due to the low O_2 supply. A 'Great Oxidation Event' occurs in the model when consumption of atmospheric oxygen via reduced gases is reduced to a value lower than the total oxygen source from organic C burial (at ~1.5×10^{13} mol O_2 equivalent). We find that

atmospheric O_2 rises by several orders of magnitude to ~0.06 – 0.25 PAL, broadly consistent with several estimates for the mid-Proterozoic (0.01 – 0.1 PAL (*37*)), and the O_2 balance is primarily controlled by oxidative weathering (*30*). Deep ocean oxygen concentration also rises to around 1% of the modern value, whilst the proximal and distal shelf environments remain anoxic, as O_2 diffusion from the atmosphere is not sufficient to outweigh oxygen demand.

Under a further decrease in reductant input, shelf environments undergo rapid oxygenation events. Here, gradually rising atmospheric oxygen concentrations cause a step-change in water column redox due to the positive feedback between bottom-water oxygen concentration and net P burial. Gradual ventilation of shelf bottom waters results in greater net removal of P, reducing overall O_2 demand and promoting further oxygenation. As the input of reduced gas declines, this transition happens first in the proximal shelf, and then in the distal shelf environment, as the latter is more strongly buffered against oxygenation due to upwelling of P from anoxic deeper waters. Finally, as reductant input declines further, the deep ocean becomes fully-oxygenated (reductant input of $< 0.5 \times 10^{13}$ mol O_2 equivalent). The positive feedback between dissolved O_2 concentration and net P burial again causes a rapid transition. In our model, the deep ocean is oxygenated when atmospheric O_2 reaches 0.7-0.8 PAL, which is consistent with values reported in other studies (*38*).

Figure 3c demonstrates the degree of sedimentary P recycling in the model (shown as C_{org}/P_{org}). These changing ratios reflect the positive feedbacks between bottom-water redox and P recycling. This P recycling is dependent only on the extent of bottom water anoxia and thus the model predicts a significant degree of recycling prior to the 'GOE'. However, under global ferruginous conditions in the early Archean, P may have been more effectively trapped in the sediment (*29*) (See SI for a test of this). Nevertheless, this would ultimately help to stabilize O_2 at low levels by reducing surface ocean productivity.

The oxygenation of the distal shelf environment has the potential for oscillatory behavior ('limit cycles'), denoted by the break in steady state lines in Fig. 3. Here, the oxygenation of the entire shelf environment results in a large reduction in overall organic carbon burial rates (as the shelves are the major locus of C_{org} burial). Over geological timescales, this reduction in carbon burial sufficiently reduces the O_2 content of the atmosphere to return the shelves to anoxia. Figure 4 shows this cyclic response of the model under reductant inputs of 1 and 2.5 × 10^{13} mol O_2 equivalent yr^{-1}. The cyclic regime includes temporary oxygenation of both the distal shelf and the deep ocean, as the rapid oxygenation event results in increased supply of oxic water via down-welling. These Ocean Oxygenation Events (OOEs) last between 2 – 5 Myrs for the range of redox dependencies tested in the model, and occur on approximate 5 – 20 Myr timescales.

Our model demonstrates that gradual oxygenation of Earth's surface over time results in distinct oxygenation events. This occurs because in our model the atmosphere, continental shelves, and deep ocean act as distinct 'compartments' of the Earth system (*39, 40*), which are controlled by local, rather than global feedbacks (*41*). Firstly, a 'Great Oxidation' of the atmosphere occurs, followed by oxygenation of nearshore shelf environments, and then distal shelf environments. This oxygenation of the whole shelf is manifest as an oscillating solution, which would likely lead to a series of Ocean Oxygenation Events. Finally, the deep ocean becomes resiliently oxygenated. This sequence of events tracks the apparent oxygenation history of the Earth as recorded by multiple redox proxies, including cycling between oxic and anoxic deep ocean states during the Neoproterozoic and early Paleozoic (*6*). Our model of course neglects some potentially-stabilizing negative feedbacks, such as the climate-silicate weathering link, although models that do include these processes still exhibit rapid shifts in marine anoxia e.g.(*42*).

In Fig. 5 we examine the potential for our model to recreate Earth's oxygenation history by performing transient model simulations under a continuous decline in reductant input constrained by mantle thermal evolution (*43*). In light of the potential for high Archean reductant availability and outgassing, and considering the relatively high rate of O_2 production in our model, we test starting fluxes of 4.5×10^{13} mol O_2 equivalent yr^{-1} at 4 Ga (*35, 43*). With or without the inclusion of open water P scavenging, the model is able to recreate the broad observed pattern of atmospheric and oceanic oxygenation over Earth history. This includes a 'Great Oxidation' of the atmosphere at around 2.5-2 Ga, and unstable oxygenation of the deeper ocean starting at around 1 Ga, which continues until permanent oxygenation of the deep ocean is established at around 0.7 – 0.4 Ga.

We compare our model results with a compilation of phosphorus concentrations from marine shales (*29*) (Fig. 5). The data show an approximate four-fold increase in P weight percent between the Precambrian and Phanerozoic baselines, and this corresponds to an increase in P burial rate in the model shelf environment between the 'Proterozoic' and 'oxygenated ocean' states. Our model does not calculate sediment phosphorus weight percentages, but does produce an upwards baseline shift in shelf sedimentary phosphorus burial rate, which is qualitatively consistent with the data. This increase in P burial is much greater when open ocean scavenging is included, as the shutdown of scavenging upon deep ocean oxygenation results in significantly more P remaining in the system, in exactly the manner described by Reinhard et al. (2017). Interestingly, we also note a 2-4 fold increase in shelf P burial rates when the model does not include open-ocean scavenging. This occurs simply because more P is trapped in the sediments when the shelves become oxygenated.

It is important to note that the reductant-driven oxygenation of the surface system that we analyze here, although plausible, is only one way in which to drive gradual net surface redox changes over time. Others include the long-term build-up of organic carbon in the crust

(*13, 43*), the escape of hydrogen to space (*44*) or a gradually increasing supply of phosphorus to the ocean. Net redox changes driven by continual removal of hydrogen or C_{org} from Earth's surface should operate in a similar way to the addition of reduced gases that we explore here. Interestingly, in these model runs, under a fixed present-day rate of riverine phosphate delivery and no scavenging flux, the model predicts a declining inventory of ocean P and declining rates of productivity and carbon burial over Earth history, as sedimentary P recycling is curtailed (see Figure S4 for full details). When scavenging is considered, the P inventory and overall C_{org} burial rates are broadly static through early Earth history and increase slightly when the deep ocean is oxygenated. Both model outputs reproduce the increasing P concentrations in shales through time (*29*), and although we cannot produce a $\delta^{13}C$ record with this model (as it lacks an inorganic carbon cycle), it would likely be consistent with the geological record; firstly because the model can produce either an increase or decrease in C_{org} burial, and secondly because ocean $\delta^{13}C$ is buffered by the adjustment of oxidative weathering rates at low O_2 (*30*), and by higher rates of inorganic carbon degassing and deposition on the Early Earth (*45*). Nevertheless, although phosphorus input over Earth history is highly uncertain (*46*) it is quite commonly assumed that the P inventory, along with productivity and carbon burial rates, have increased substantially over time. Thus, in the SI we re-run our model under a varying riverine P input and show that the stepwise oxygenation events are indeed reproducible when Earth's gradual redox shift is driven by a steady increase in P supply to the oceans.

We demonstrate here that relationships between the global phosphorus, carbon and oxygen cycles are fundamental to understanding the oxygenation history of the Earth. Our model confirms that observed 'oxygenation events' through Earth history may be driven by well-defined internal system feedbacks between these cycles, without the requirement for extensive external forcings. The results of this analysis are wide-reaching. It appears that oxygenation of the Earth's surface did not require any biological advances beyond simple

photosynthetic cyanobacteria, and was simply a matter of time, which drastically increases the possibility of high-O_2 worlds existing elsewhere.

References and Notes:

1. J. Farquhar, H. Bao, M. Thiemens, Atmospheric Influence of Earth's Earliest Sulfur Cycle. *Science* **289**, 756-758 (2000).
2. N. J. Planavsky *et al.*, Low Mid-Proterozoic atmospheric oxygen levels and the delayed rise of animals. *Science* **346**, 635-638 (2014).
3. D. S. Hardisty *et al.*, Perspectives on Proterozoic surface ocean redox from iodine contents in ancient and recent carbonate. *Earth and Planetary Science Letters* **463**, 159-170 (2017).
4. S. W. Poulton, D. E. Canfield, Ferruginous Conditions: A Dominant Feature of the Ocean through Earth's History. *Elements* **7**, 107-112 (2011).
5. L. Och, G. Shields-Zhou, The Neoproterozoic oxygenation event: Environmental pertubations and biogeochemical cycling. *Earth-Science Reviews* **110**, 26-57 (2012).
6. S. H. Sahoo *et al.*, Oceanic oxygenation events in the anoxic Ediacaran ocean. *Geobiology* **14**, 457-468 (2016).
7. A. J. Krause *et al.*, Stepwise oxygenation of the Paleozoic atmosphere. *Nature Communications* **9**, 4081 (2018).
8. N. J. Butterfield, Early evolution of the Eukaryota. *Palaeontology* **58**, 5-17 (2015).
9. J. J. Brocks *et al.*, The rise of algae in the Cryogenian oceans and the emergence of animals. *Nature* **548**, 578-581 (2017).
10. K. M. Meyer, A. Ridgwell, J. L. Payne, The influence of the biological pump on ocean chemistry: implications for long-term trends in marine redox chemistry, the global carbon cycle, and marine animal ecosystems. *Geobiology* **14**, 207-219 (2016).

11. T. M. Lenton, R. A. Boyle, S. W. Poulton, G. A. Shields-Zhou, N. J. Butterfield, Co-evolution of eukaryotes and ocean oxygenation in the Neoproterozoic era. *Nature Geoscience* **7**, 257-265 (2014).

12. L. R. Kump, M. E. Barley, Increased subaerial volcanism and the rise of atmospheric oxygen 2.5[thinsp]billion years ago. *Nature* **448**, 1033-1036 (2007).

13. C.-T. A. Lee *et al.*, Two-step rise of atmospheric oxygen linked to the growth of continents. *Nature Geoscience* **9**, 417-424 (2016).

14. I. H. Campbell, C. M. Allen, Formation of supercontinents linked to increases in atmospheric oxygen. *Nature Geoscience* **1**, 554-558 (2008).

15. F. Horton, Did phosphorus derived from the weathering of large igneous provinces fertilize the Neoproterozoic ocean? *Geochemistry, Geophysics, Geosystems* **16**, 1723-1738 (2015).

16. A. H. Knoll, M. A. Nowak, The timetable of evolution. *Science Advances* **3**, (2017).

17. T. M. Lenton, S. J. Daines, The effects of marine eukaryote evolution on phosphorus, carbon and oxygen cycling across the Proterozoic-Phanerozoic transition. *Emerging Topics in Life Sciences*, (2018).

18. C. Goldblatt, T. M. Lenton, A. J. Watson, Bistability of atmospheric oxygen and the Great Oxidation. *Nature* **443**, 683-686 (2006).

19. M. W. Claire, D. C. Catling, K. J. Zahnle, Biogeochemical modelling of the rise in atmospheric oxygen. *Geobiology* **4**, 239-269 (2006).

20. T. A. Laakso, D. P. Schrag, A theory of atmospheric oxygen. *Geobiology* **15**, 366-384 (2017).

21. T. A. Laakso, D. P. Schrag, Regulation of atmospheric oxygen during the Proterozoic. *Earth and Planetary Science Letters* **388**, 81-91 (2014).

22. T. Tyrrell, The relative influences of nitrogen and phosphorus on oceanic primary production. *Nature* **400**, 525-531 (1999).

23. M. D. Krom, R. A. Berner, The diagenesis of phosphorus in a nearshore marine sediment. *Geochimica et Cosmochimica Acta* **45**, 207-216 (1981).

24. K. C. Ruttenberg, R. A. Berner, Authigenic apatite formation and burial in sediments from non-upwelling, continental margin environments. *Geochimica et Cosmochimica Acta* **57**, 991-1007 (1993).

25. T. Jilbert, C. P. Slomp, Iron and manganese shuttles control the formation of authigenic phosphorus minerals in the euxinic basins of the Baltic Sea. *Geochimica et Cosmochimica Acta* **107**, 155-169 (2013).

26. P. Van Cappellen, E. D. Ingall, Benthic phosphorus regeneration, net primary production, and ocean anoxia: A model of the coupled marine biogeochemical cycles of carbon and phosphorus. *Paleoceanography* **9**, 677-692 (1994).

27. C. P. Slomp, J. Thomson, G. J. De Lange, Enhanced regeneration of phosphorus during formation of the most recent eastern Mediterranean sapropel (S1). *Geochimica et Cosmochimica Acta* **66**, 1171-1184 (2002).

28. I. Tsandev, C. P. Slomp, Modelling phosphorus cycling and carbon burial during Cretaceous Oceanic Anoxic Events. *Earth and Planetary Science Letters* **286**, 71-79 (2009).

29. C. T. Reinhard *et al.*, Evolution of the global phosphorus cycle. *Nature* **541**, 386-389 (2017).

30. S. J. Daines, B. J. W. Mills, T. M. Lenton, Atmospheric oxygen regulation at low Proterozoic levels by incomplete oxidative weathering of sedimentary organic carbon. *Nature Communications* **8**, (2017).

31. I. C. Handoh, T. M. Lenton, Periodic mid-Cretaceous oceanic anoxic events linked by oscillations of the phosphorus and oxygen biogeochemical cycles. *Global Biogeochemical Cycles* **17**, 1092 (2003).

32. C. P. Slomp, P. Van Cappellen, The global marine phosphorus cycle: sensitivity to oceanic circulation. *Biogeosciences* **4**, 155-171 (2007).

33. I. Tsandev, C. P. Slomp, P. Van Cappellen, Glacial-interglacial variations in marine phosphorus cycling: Implications for ocean productivity. *Global Biogeochemical Cycles* **22**, (2008).

34. P. Kharecha, J. F. Kasting, J. Siefert, A coupled atmosphere-ecosystem model of the early Archean Earth. *Geobiology* **3**, 53-76 (2005).

35. J. Krissansen-Totton, G. N. Arney, D. C. Catling, Constraining the climate and ocean pH of the early Earth with a geological carbon cycle model. *PNAS* **115**, 4105-4110 (2018).

36. A. A. Pavlov, J. F. Kasting, Mass-independent fractionation of sulfur isotopes in Archean sediments: strong evidence for an anoxic Archean atmosphere. *Astrobiology* **2**, 27-41 (2002).

37. D. C. Catling, M. W. Claire, How Earth's atmosphere evolved to an oxic state: a status report. *Earth and Planetary Science Letters* **237**, 1-20 (2005).

38. E. A. Sperling *et al.*, Statistical analysis of iron geochemical data suggests limited late Proterozoic oxygenation. *Nature* **523**, 451-454 (2015).

39. K. Wallmann, Feedbacks between oceanic redox states and marine productivity: A model perspective focused on benthic phosphorus cycling. *Global Biogeochemical Cycles* **17**, n/a-n/a (2003).

40. W. S. Broecker, T. H. Peng, *Tracers in the Sea*. (Eldigio Press, New York, 1982), pp. 690.

41. C. J. Bjerrum, D. E. Canfield, T. W. Dahl, Chasing Neoptoerozoic Atmospheric Oxygen Ghosts. American Geophysical Union, Fall Meeting, 2016.

42. T. M. Lenton, S. J. Daines, B. J. W. Mills, COPSE reloaded: An improved model of biogeochemical cycling over Phanerozoic time. *Earth-Science Reviews* **178**, 1-28 (2018).

43. J. M. Hayes, J. R. Waldbauer, The carbon cycle and assocaited redox process through time. *Philos Trans R Soc* **361**, 931-950 (2006).

44. D. C. Catling, K. J. Zahnle, C. P. McKay, Biogenic Methane, Hydrogen Escape, and the Irreversible Oxidation of Early Earth. *Science* **293**, 839-843 (2001).

45. G. A. Shields, B. J. W. Mills, Tectonic controls on the long-term carbon isotope mass balance. *PNAS* **114**, 4318-4323 (2017).

46. B. Mills, T. M. Lenton, A. J. Watson, Proterozoic oxygen rise linked to shifting balance between seafloor and terrestrial weathering. *Proc Natl Acad Sci U S A* **111**, 9073-9078 (2014).

47. T. W. Lyons, C. T. Reinhard, N. J. Planavsky, The rise of oxygen in Earth's early ocean and atmosphere. *Nature* **506**, 307-315 (2014).

48. K. C. Ruttenberg, Reassessment of the oceanic residence time of phosphorus. *Chemical Geology* **107**, 405-409 (1993).

49. A. J. Watson, T. M. Lenton, B. J. W. Mills, Ocean deoxygenation, the global phosphorus cycle and the possibility of human-caused large-scale ocean anoxia. *Philosophical Transactions of the Royal Society A: Mathematical, Physical and Engineering Sciences* **375**, (2017).

50. E. D. Ingall, R. M. Bustin, P. Van Cappellen, Influence of water column anoxia on the bruial and preservation of carbon and phosphorus in marine shales. *Geochimica et Cosmochimica Acta* **57**, 303-316 (1993).

51. S. W. Poulton, Early Phosphorus Redigested. *Nature Geoscience* **10**, 75-76 (2017).

52. N. M. Bergman, T. M. Lenton, A. J. Watson, COPSE: A new model of biogeochemical cycling over Phanerozoic time. *American Journal of Science* **304**, 397-437 (2004).

Acknowledgments:

We thank C. Slomp and K. Wallmann for sending computer code, we also thank the reviewers of this work for constructive and useful comments.

Funding: L.J.A is funded by a Leeds Anniversary Research Scholarship. B.J.W.M acknowledges support from a University of Leeds Academic Fellowship. S.W.P. acknowledges support from a Leverhulme Research Fellowship and a Royal Society Wolfson Research Merit Award. B.J.W.M and S.W.P are funded by the UK Natural Environment Research Council (NE/R010129/1 and NE/S009663/1).

Author contributions: L.J.A and B.J.W.M designed the research and developed the model. L.J.A performed model runs. All authors wrote the manuscript.

Competing interests: Authors declare no competing interests.

Data and materials availability: All data is available in the main text or the supplementary materials. Model code and output data are available from the corresponding author on reasonable request.

Supplementary Materials:

Materials and Methods

Figures S1-S4

Tables S1-S3

References (48-52)

Figures:

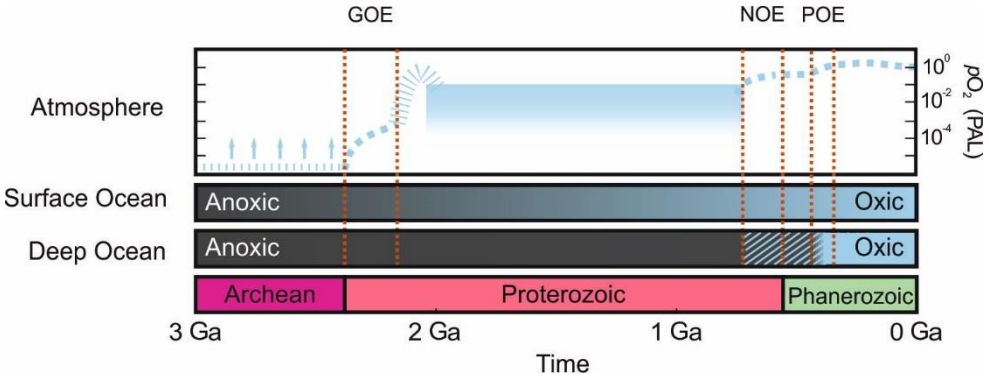

Figure 1. Redox history of the Earth. *Atmospheric O_2 based on (47). GOE – Great Oxidation Event, NOE – Neoproterozoic Oxygenation Event, POE – Paleozoic Oxygenation Event. Ga – Billion Years. Crosshatch indicates variable deep ocean redox between the start of the NOE and the POE. See text for summary and references.*

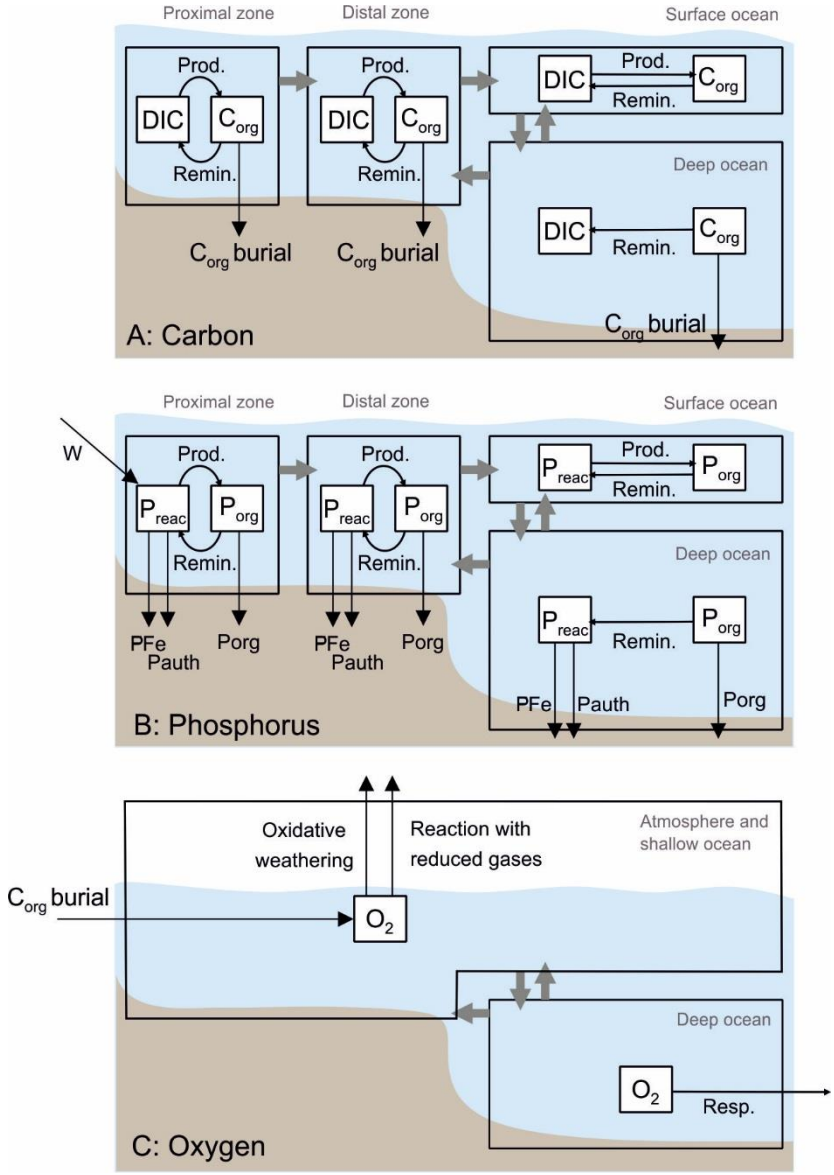

Figure 2. Ocean and atmosphere box model. *Clear boxes show hydrospheric reservoirs and grey arrows denote mixing between them. White boxes show chemical reservoirs and black arrows denote biogeochemical fluxes. (A) Carbon cycle: C exists as dissolved inorganic carbon (DIC) or organic carbon (C_{org}). (B) Phosphorus cycle: P exists as soluble reactive phosphorus (P_{reac}) and particulate organic phosphorus (P_{org}). (C) Oxygen cycle. Single oxygen reservoir encompasses all ocean boxes that exchange with the atmosphere. See text for full description, and methods and SI for equations.*

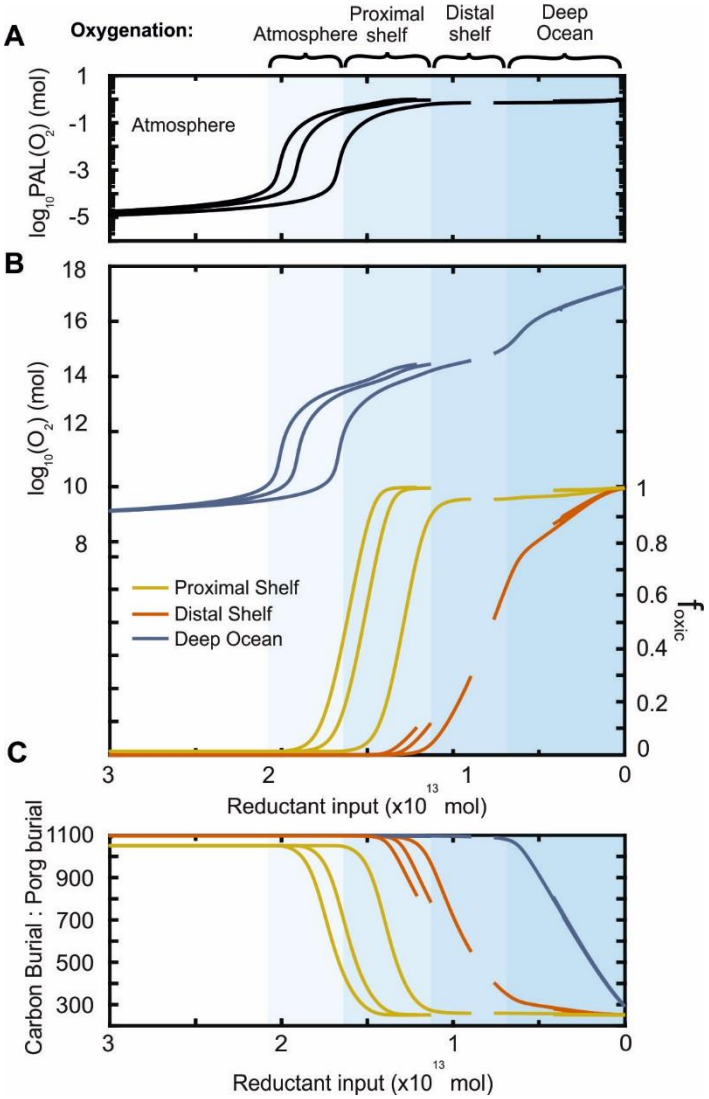

Figure 3. Model stable solutions with respect to overall surface redox state. *The model is run to steady state for changes to the reduced gas input rate. (A) Atmospheric O_2 reservoir. (B) Deep ocean O_2 reservoir (mol) and shelf 'oxic fraction' of seafloor (f_{oxic}). (C) Molar carbon and phosphorus burial ratio in sediments. Three lines for each zone represent different choices of redox dependence for P burial fluxes (see text). Breaks in solid lines indicate periods where no stable solution exists, in these parameter spaces the model produces an oscillating solution.*

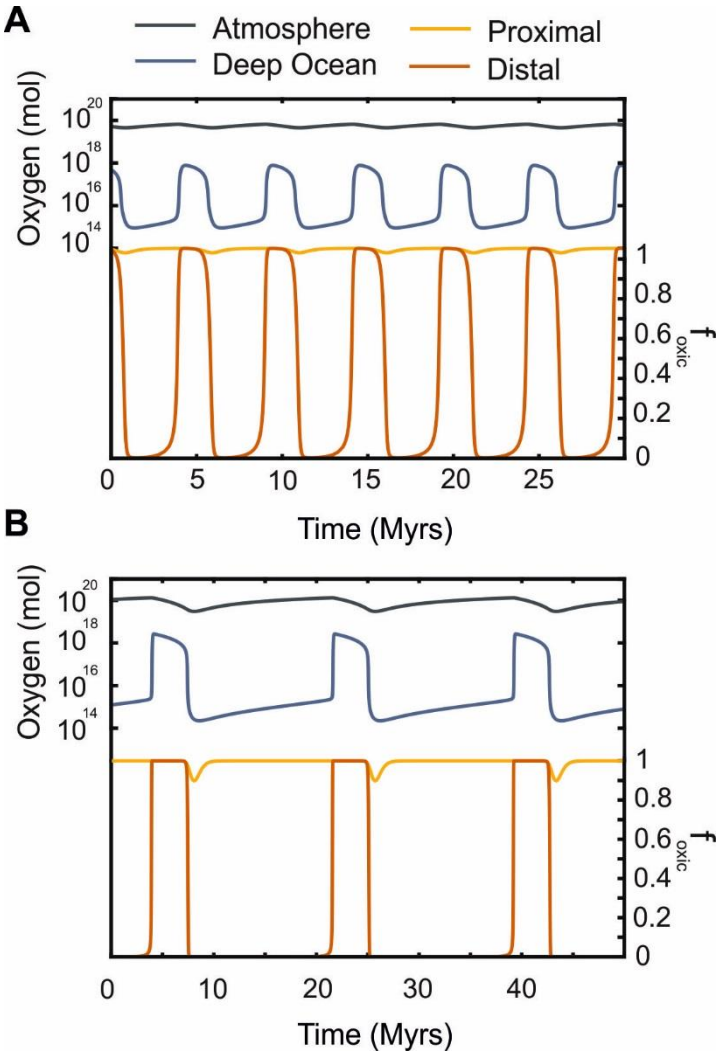

Figure 4. Oscillating redox solutions. *Transient model responses, demonstrating limit cycles of frequency ~5-20 Myrs. (A) Conservative redox dependency for deep ocean P burial terms (50% - P_{auth}, 25% - P_{org}) with 1×10^{13} moles of oxygen consumption. (B) Stronger redox dependencies following Tsandev and Slomp, 2009 (90% - P_{auth}, 50% - P_{org}) with 2.5×10^{13} moles of oxygen consumption.*

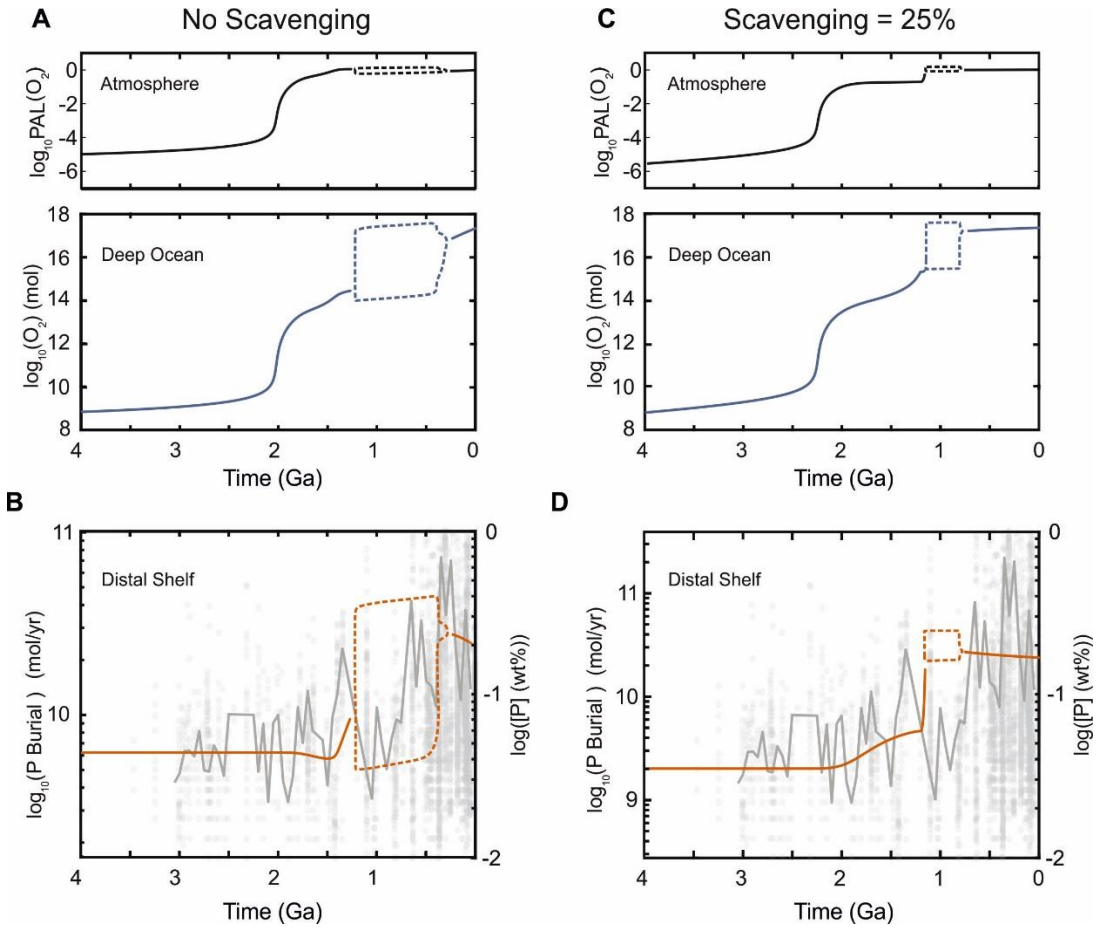

Figure 5. Possible O_2 evolution over Earth history. *Model is run for 4 Gyrs subject to a decrease in reductant input – illustrative of a gradual shift in net redox, and demonstrating possible evolution of surface O_2 levels. Dotted boxes represent the boundaries of limit cycles in the solution. (A, C) Atmosphere and deep ocean O_2 abundances. (B, D) Total shelf P burial rates (red, left axis) compared to phosphorus abundance in marine shales (Reinhard et al., 2017; right axis). Grey line shows 50 Myr binned moving average through compilation data. (A, B) No iron-bound scavenging and redox dependencies of 50% - P_{auth}, 25% - P_{org} following Slomp and Van Cappellen (2007) with a starting O_2 consumption via reductants of 45×10^{12} mol/yr and a linear decrease. (C, D) Iron-bound scavenging included with a maximum rate of 5×10^{10} mol P/yr. Stronger redox dependencies, following Tsandev and Slomp, (2009) (90% - P_{auth}, 50% - P_{org}). Starting O_2 consumption via reductants was 45×10^{12} mol/yr and an exponential decrease.*

Science
AAAS

Supplementary Materials for

Stepwise Earth oxygenation is an inherent property of global biogeochemical cycling

Lewis J. Alcott[1]*, Benjamin J. W. Mills[1], Simon W. Poulton[1]

[1]School of Earth and Environment, University of Leeds, Leeds LS2 9JT, UK.

Correspondence to: eelja@leeds.ac.uk

This PDF file includes:

Materials and Methods

Model summary

The box model framework presented here is modified from Slomp and Van Cappellen (2007), Tsandev et al. (2008) and Tsandev and Slomp (2009). All model equations are shown in tables S1-S3 and are numbered sequentially in those tables, and the key equations are discussed below. Equations which we have modified or added are denoted as such in tables S1-S3. The model includes 4 ocean boxes, which include P, C_{org} and O cycles, and one atmosphere box, which only considers oxygen. The continental shelves are separated into proximal and distal zones, where the proximal shelf is directly influenced by riverine input, and the distal shelf is influenced by coastal upwelling (*39*). The open ocean is divided into a surface and deep ocean, with the deep ocean including the continental slope. A key modification of the previous model is that redox-dependent P burial is now included within all areas of the model that contain a burial term, as we now vary the redox state within all the environments of deposition within the model. The P burial phases considered in the model consist of organic P (P_{org}), iron oxide bound P (P_{Fe}) and authigenic phosphorus, modelled as calcium fluorapatite (P_{auth}). The partitioning of these sinks corresponds to preindustrial interglacial conditions, with the sinks for P_{org}, P_{Fe} and P_{auth} accounting for 25%, 25% and 50% of the total burial flux, respectively (*48*).

The organic carbon cycle follows Slomp and Van Cappellen (2007). Respiration of oxygen is only explicitly calculated in the deep ocean and is assumed to be linearly dependent on the availability of organic carbon, with a dependence on oxygen availability expressed via a Monod function:

$$OResp = kResp \cdot \left(\frac{\boldsymbol{C_{DP}}}{RedOC}\right) \cdot \frac{O_{DP}}{(kmO_2 + O_{DP})} \qquad (43)$$

where $kResp$ is a constant to adjust for present day values, $\boldsymbol{C_{DP}}$ is the normalized amount of organic carbon in the deep ocean at present day, $RedOC$ is the O:C ratio (138:106), O_{DP} is the quantity of oxygen (moles) in the deep ocean, and kmO_2 is the Monod constant, below which respiration ceases to function.

Respiration of organic carbon is calculated in the same manner but without the inclusion of the Redfield adjustment or the Monod function, this embodies the assumption that respiration will continue anaerobically once oxygen is depleted. The burial of organic carbon in the proximal and distal boxes is proportional to the amount of organic carbon production within the box, scaled to present day values. The burial of organic carbon in the deep ocean is calculated from the organic phosphorus burial flux and the C_{org}:P_{org} ratio within the sediment. Both of these approaches follow the original models.

$$POCbur_{DP} = POPbur_{DP} \cdot \frac{(CP_{anoxic} \cdot CP_{oxic})}{([\boldsymbol{O_{DP}}] \cdot CP_{anoxic}) + ((1 - [\boldsymbol{O_{DP}}]) \cdot CP_{oxic})} \quad (41)$$

where $POPbur_{DP}$ is the quantity of organic bound P (moles) buried in the deep ocean, $[\boldsymbol{O_{DP}}]$ is the concentration of oxygen in the deep ocean normalized to present day, with CP_{anoxic} and CP_{oxic} being the C:P ratios for anoxic and oxic conditions as used by Slomp and Van Cappellen (2007).

The oxygen content of the surface ocean boxes in contact with the atmosphere are assumed to vary according to the normalized atmospheric oxygen content. The proximal and distal zones also include the f_{anoxic} parameter. This parameter, as determined by Watson et al (2017), is analogous to the Degree of Anoxia (DOA) (*28*), and indicates the fraction of the ocean floor in that reservoir that can be considered anoxic:

$$f_{anoxic} = \frac{1}{(1 + e^{(-k_{anox} \cdot (kU \cdot \boldsymbol{P_x} - \boldsymbol{O_A})})} \quad (75)$$

where k_{anox} = 10, kU = 0.4, $\boldsymbol{P_x}$ is the normalised amount of Soluble Reactive Phosphorus available within the relevant ocean box ($\boldsymbol{x = P, D}$), and $\boldsymbol{O_A}$ is the amount of oxygen within the atmosphere, normalized to present day values (*49*). For the present day, f_{anoxic} is calculated to be 0.0025 (*49*). This f_{anoxic} fraction is used primarily to introduce redox dependent burial of P within the proximal and distal zones.

The sorption of P to ferric iron oxides is considered to be redox dependent. Under anoxic conditions, it is assumed that the reduction of these iron oxides occurs leads to less P sorption and ultimately less P_{Fe} burial. A linear relationship between the present day flux of P_{Fe} and the normalised

amount of oxygen is used to calculate the burial of P_{Fe} within the deep ocean. P_{Fe} burial is linearly dependent on the amount of SRP available within the proximal zone, and in the distal zone it is related to both the availability of SRP and the value of f_{anoxic}, following Tsandev and Slomp (2009) and Watson et al (2017):

$$PFe_{DP} = kFeP_{DP} \cdot [\boldsymbol{O_{DP}}] \quad (66)$$

$$PFe_P = kFeP_P \cdot P_P \quad (52)$$

$$PFe_D = kFeP_D \cdot P_D \cdot (1 - fanoxic_{dist}) \quad (57)$$

where $kFeP_{DP}$ is the normalised present day burial flux of P_{Fe} for the respective reservoir and P_P and P_D represent the quantity of soluble reactive phosphorus in the proximal and distal zones, respectively. During early diagenesis, P is preferentially released with respect to organic carbon during anaerobic remineralization by bacteria (*23, 50*), leading to sedimentary C:P ratios much greater than the molar C:P Redfield ratio of 106:1. P release also occurs under oxic conditions, but to a lesser extent. 25% of the buried POP (Particulate Organic Phosphorus) is redox dependent in our standard model, as in Slomp and Van Cappellen (2007). Once this value has been calculated based on the amount of export production, a C:P ratio is determined based upon the amount of oxygen present (or f_{anoxic} parameter) relative to standard oxic and anoxic C:P ratios (*26*) (Table S2). These values are 250 and 1100 for oxic and anoxic conditions, respectively (CP_{oxic} and CP_{anoxic}) (*32, 49*).

$$POPbur_{DP} = kPOPbur_{DP} \cdot \left(\frac{xp_{SDP}}{CP_{oxic}}\right) \cdot (0.75 + (0.25 \cdot [\boldsymbol{O_{DP}}])) \quad (74)$$

$$POPbur_P = kcbur_P \cdot PP_P \cdot CPratio_{proximal} \quad (69)$$

$$POPbur_D = kPOPbur_D \cdot (PP_D + xp_{PD}) \cdot CPratio_{distal} \quad (71)$$

where $kPOPbur_x$ is the present day value for Porg burial for the respective reservoir, xp_{SDP} is the export production from surface waters to the deep ocean, PP_P and PP_D represent primary production (moles of carbon) in the proximal and distal zones, respectively and $kcbur_x$ quantifies the flux of organic carbon burial within the respective reservoir.

P_{auth} is formed from the precipitation and ultimate burial of authigenic carbonate fluorapatite (*24*). This is typically considered the major sink for P that is released from organic matter (*24*), however recent work is revealing other key contributors (e.g. vivianite (*25*)). The P release under an anoxic water column typically occurs in the water column or close to the sediment water interface, allowing a significant proportion to be recycled back to the water column (*27*). Therefore, as in previous iterations of this model, we assume a redox dependence on the formation of P_{auth}. However, there were times in Earth history when widespread anoxic ferruginous conditions may have hampered P recycling, due to effective sequestration of P in association with Fe minerals (*29*), although this concept has been questioned (*51*). We therefore tested the effect of different redox dependencies on P recycling, and test the inclusion of a P scavenging flux. In our standard model, P_{auth} formation is considered to be linearly dependent on the quantity of POP mineralization within the overlying ocean box (*32*). A redox dependency on P_{auth} is also included into the distal zone, where it is linearly proportional to f_{anoxic} and the rate of respiration in the distal zone (as in Tsandev and Slomp (2009)). Authigenic P burial in the proximal zone is not redox dependent and is related to the mineralized POP flux and the quantity of POP present at that time step, where we allow 25% to be redox dependent:

$$Pauth_{DP} = kCaP_{DP} \cdot POPmin_{DP} \cdot (0.75 + (0.25 \cdot [\boldsymbol{O_{DP}}])) \quad (67)$$

$$Pauth_P = kpmin_P \cdot OP_P \cdot kCaP_P \quad (53)$$

$$Pauth_D = kCaP_D \cdot \boldsymbol{O_D} \cdot (1 - fanoxic_{dist}) \quad (58)$$

where $kCaP_x$ is used to adjust for present day values of P_{auth} burial in the respective reservoir, $POPmin_{DP}$ is the quantity of particulate organic phosphorus that is mineralised in the deep ocean, $kpmin_p$ is a constant used to determine the quantity of organic phosphorus that is mineralised in the proximal zone, OP_P is the quantity of particulate organic phosphorus that is in the proximal zone, and $\boldsymbol{O_D}$ is the present day normalized amount of oxygen in the distal ocean.

All dissolved species are circulated based on their concentration and the associated water fluxes as in Slomp and Van Cappellen (2007). Primary production of organic carbon is linearly related to P concentration as in Slomp and Van Cappellen (2007).

Full model equations

All model equations are listed below. The model takes most fluxes directly from Slomp and Van Cappellen (2007) and Tsandev and Slomp (2009), adding some equations from Bergman et al. (2004). We modify the model of Slomp and Van Cappellen (2007) by allowing the oxygen concentration in the boxes in contact with the atmosphere to vary and adding and explicitly calculated atmospheric reservoir of oxygen. Tsandev and Slomp (2009) also developed upon this model and included a redox dependent phosphorus cycle on the proximal and distal shelf, which we include here subject to the following alterations: We altered the redox parameter used by Tsandev and Slomp (2009) to the revised parameter (f_{anoxic}) used by Watson et al. (2017). In addition to these changes we also removed phosphorus associated with fish bones from the model.

Table S1: Present day reservoirs with the corresponding flux equations. The models steady state present day values are presented below in addition to the flux equations relative both to the respective fluxes and reservoirs.

Reservoir	Eq No.	Label	Initial Size (moles)	Differential Equation	Source
Proximal Water	1	W_P	$36x10^{12}$	$River_W - circ_{PD}$	[1]
Distal Water	2	W_D	$3600x10^{12}$	$circ_{PD} + circ_{DPD} - circ_{DS}$	[1]
Surface Water	3	W_S	$4{,}983x10^{13}$	$circ_{DPS} + circ_{DS} - circ_{SDP} - Evap$	[1]
Deep Ocean Water	4	W_{DP}	$1.3x10^{18}$	$circ_{SDP} - circ_{DPS} - circ_{DPD}$	[1]
Proximal Carbon	5	C_P	$4.5x10^{12}$	$PP_P - POCmin_P - POCbur_P - xp_{PD}$	[1]
Distal Carbon	6	C_D	$243x10^{12}$	$xp_{PD} + PP_D - POCbur_D - POCmin_D - xp_{DS}$	[1]
Surface Carbon	7	C_S	$3{,}816x10^{12}$	$xp_{DS} + PP_S - POCmin_S - xp_{SDP}$	[1]
Deep Ocean Carbon	8	C_{DP}	$5.6x10^{16}$	$xp_{SD} - RespPOC - POCbur_{DP}$	[1]
Proximal Oxygen	9	O_P	$4.5x10^{12}$	$O_{P_0} \cdot \boldsymbol{O_A}$	[1]
Distal Oxygen	10	O_D	$243x10^{12}$	$O_{D_0} \cdot \boldsymbol{O_A}$	[1]
Surface Oxygen	11	O_S	$1.615x10^{16}$	$O_{S_O} \cdot \boldsymbol{O_A}$	[1]

Deep Ocean Oxygen	12	O_{DP}	$2.21x10^{17}$	$O_{SDP} - OResp - O_{DPS} - O_{DPD}$	[1]
Atmosphere Oxygen	13	O_A	$3.7x10^{19}$	$POCburT - AtmosW - genred$	[2]
Proximal SRP	14	P_P	$9.7x10^{9}$	$W_P - PPP_P + POPmin_P - PFe_P - Pauth_P - SRP_{PD}$	[1]
Distal SRP	15	P_D	$5x10^{12}$	$SRP_{PD} - PPP_D + POPmin_D - PFe_D - Pauth_D - SRP_{DS} + SRP_{DPD}$	[1]
Surface SRP	16	P_S	$47x10^{12}$	$SRP_{DS} - PPP_S + POPmin_S + SRP_{SDP} + SRP_{DPS}$	[1]
Deep Ocean SRP	17	P_{DP}	$2{,}790x10^{12}$	$SRP_{SDP} + POPmin_{DP} - PFe_P - Pauth_{DP} - SRP_{DPS} - SRP_{DPD}$	[1]
Proximal POP	18	OP_P	$4.3x10^{10}$	$PPP_P - POPmin_P - POPbur_P - POP_{PD}$	[1]
Distal POP	19	OP_D	$2.3x10^{12}$	$POP_{PD} + PPP_D - POPmin_D - POPbur_D - POP_{DS}$	[1]
Surface POP	20	OP_S	$36x10^{12}$	$POP_{DS} + PPP_S - POPmin_S - POP_{SDP}$	[1]
Deep Ocean POP	21	OP_{DP}	$530x10^{12}$	$POP_{SDP} - POPmin_{DP} - POPbur_{DP}$	[1]

Table S2: Present day flux values and corresponding equations.

Flux	Eq No.	Label	Initial flux (moles/yr)	Equation	Source
River input	22	$River_W$	$37x10^{12}$	$constant$	[1]
Proximal-Distal water	23	$circ_{PD}$	$37x10^{12}$	$constant$	[1]
Low latitude upwelling water	24	$circ_{DPD}$	$3.78x10^{14}$	$kDpD \cdot W_{DP}$	[1]
Distal- Surface ocean water	25	$circ_{DS}$	$4.15x10^{14}$	$circ_{PD} + circ_{DPD}$	[1]
High latitude upwelling water	26	$circ_{DPS}$	$3.78x10^{15}$	$kDpS \cdot W_{DP}$	[1]
High latitude downwelling water	27	$circ_{SDP}$	$4.158x10^{15}$	$kSDp \cdot W_S$	[1]
Evaporation of surface water	28	$Evap$	$37x10^{12}$	$River_W$	[1]
Proximal Primary Production OC	29	PP_P	$3.975x10^{13}$	$kPP_P \cdot \boldsymbol{P_P} \cdot RedCP$	[1]
Proximal OC mineralisation	30	$POCmin_P$	$3.277x10^{13}$	$kcmin_P \cdot \boldsymbol{C_P}$	[1]
Proximal OC burial	31	$POCbur_P$	$2.3x10^{12}$	$kcbur_P \cdot PP_P$	[1]
Proximal-Distal export prod.	32	xp_{PD}	$4.685x10^{12}$	$POP_{PD} \cdot RedCP$	[1]
Distal Primary Production OC	33	PP_D	$5.6x10^{14}$	$kPP_D \cdot \boldsymbol{P_D} \cdot RedCP$	[1]
Distal OC burial	34	$POCbur_D$	$1.7x10^{12}$	$kcbur_D \cdot (xp_{PD} + PP_D)$	[1]
Distal OC mineralisation	35	$POCmin_D$	$5.349x10^{14}$	$kcmin_D \cdot \boldsymbol{C_D}$	[1]
Distal-Surface export prod.	36	xp_{DS}	$2.811x10^{13}$	$POP_{DS} \cdot RedCP$	[1]
Surface Ocean Primary Production	37	PP_S	$3.869x10^{15}$	$kPP_S \cdot \boldsymbol{P_S}$	[1]*
Surface OC mineralisation	38	$POCmin_S$	$3.404x10^{15}$	$kcmin_S \cdot \boldsymbol{C_S}$	[1]*
Surface-Deep export prod.	39	xp_{SDP}	$4.931x10^{14}$	$kxp_{SDP} \cdot (xp_{DS} + PP_S)$	[1]*
OC Respiration	40	$RespPOC$	$4.921x10^{14}$	$kResp \cdot \boldsymbol{C_{DP}}$	[1]*
Deep Ocean OC burial	41	$POCbur_{DP}$	$1 x10^{12}$	$POPburd_{DP} \cdot \frac{(CP_{anoxic} \cdot CP_{oxic})}{([\boldsymbol{O_{DP}}] \cdot CP_{anoxic}) + ((1 - [\boldsymbol{O_{DP}}]) \cdot CP_{oxic})}$	[1]*

Surface-Deep oxygen downwelling	42	O_{SDP}	1.347x10^{15}	$circ_{SDP} \cdot [O_s]$	[1]*
Oxygen Respiration	43	$OResp$	6.403x10^{14}	$kResp \cdot (\frac{\boldsymbol{C_{DP}}}{RedOC}) \cdot (\frac{O_{DP}}{(kmO_2 + O_{DP})})$	[1]*
Deep-Surface oxygen upwelling	44	O_{DPS}	6.426x10^{14}	$circ_{DPS} \cdot [O_{DP}]$	[1]
Deep-Distal oxygen upwelling	45	O_{DPD}	6.426x10^{13}	$circ_{DPD} \cdot [O_{DP}]$	[1]
Total OC burial	46	$POCburT$	5x10^{12}	$POCbur_P + POCbur_D + POCbur_{DP}$	[4]
Oxidative Weathering	47	$AtmosW$	5x10^{12}	$kAtmosW \cdot (\sqrt{\boldsymbol{O_A}})$	[4]
Oxygen consumption via reduced gases	48	$genred$	0	Varied in ms figs 3-5 fixed in figs S1, S4 panels g-i	[4]
Riverine P input	49	W_P	9x10^{10}	Fixed in ms figs 3-5, varied in figs S1, S4 panels g-i.	[1]
Proximal Primary Production (P)	50	PPP_P	3.75x10^{11}	$\frac{PP_P}{RedCP}$	[1]
Proximal POP mineralisation	51	$POPmin_P$	3.216x10^{11}	$\boldsymbol{OP_P} \cdot kpmin_P$	[4]
Proximal Iron bound P burial	52	PFe_P	8.973x10^{9}	$kFeP_P \cdot P_P$	[4]
Proximal Authigenic P burial	53	$Pauth_P$	1.768x10^{10}	$kpmin_P \cdot OP_P \cdot kCaP_P$	[4]
Proximal-Distal SRP transport	54	SRP_{PD}	9.969x10^{9}	$circ_{PD} \cdot [P_P]$	[4]
Distal Primary Production (P)	55	PPP_D	5.283x10^{12}	$\frac{PP_D}{RedCP}$	[1]
Distal POP mineralisation	56	$POPmin_D$	5.055x10^{12}	$\boldsymbol{OP_P} \cdot kpmin_D$	[4]
Distal Iron bound P burial	57	PFe_D	6.762x10^{9}	$kFeP_D \cdot P_D \cdot (1 - fanoxic_{dist})$	[3]
Distal Authigenic P burial	58	$Pauth_D$	1.032x10^{10}	$kCaP_D \cdot \boldsymbol{O_D} \cdot (1 - fanoxic_{dist})$	[3]
Distal-Surface SRP transport	59	SRP_{DS}	5.764x10^{11}	$circ_{DS} \cdot [P_D]$	[1]
Deep-Distal SRP transport	60	SRP_{DPD}	8.113x10^{11}	$circ_{DPD} \cdot [P_{DP}]$	[1]
Surface Ocean Primary Production (P)	61	PPP_S	3.650x10^{13}	$\frac{PP_S}{RedCP}$	[1]*
Surface POP mineralisation	62	$POPmin_S$	3.173x10^{13}	$OP_S \cdot kpmin_S$	[4]
Surface-Deep SRP transport	63	SRP_{SDP}	3.922x10^{12}	$circ_{SDP} \cdot [P_S]$	[1]
Deep-Surface SRP transport	64	SRP_{DPS}	8.113x10^{12}	$circ_{DPS} \cdot [P_{DP}]$	[1]
Deep POP mineralisation	65	$POPmin_{DP}$	5.028x10^{12}	$OP_{DP} \cdot kpmin_{DP}$	[4]
Deep Iron bound P burial	66	PFe_{DP}	6.75x10^{9}	$kFeP_{DP} \cdot [\boldsymbol{O_{DP}}]$	[3]
Deep Authigenic P burial	67	$Pauth_{DP}$	1.953x10^{10}	$kCaP_{DP} \cdot POPmin_{DP} \cdot (0.75 + (0.25 \cdot [\boldsymbol{O_{DP}}]))$	[3]
CP ratio for respective box	68	$CPratio$	250 (oxic) 1100 (anoxic)	$\left(\frac{1 - fanoxic_x}{CP_{oxic}}\right) + (\frac{fanoxic_x}{CP_{anoxic}})$	[1]

Proximal POP burial	69	$POPburd_P$	$9.182x10^9$	$kcbur_P \cdot PP_P \cdot CPratio_{proximal}$	[4]
Proximal-Distal POP transport	70	POP_{PD}	$4.419x10^{10}$	$circ_{PD} \cdot [OP_P]$	[4]
Distal POP burial	71	$POPbur_D$	$6.800x10^9$	$kPOPbur_d \cdot (PP_D + xp_{PD}) \cdot CPratio_{distal}$	[4]
Distal-Surface POP transport	72	POP_{DS}	$2.651x10^{11}$	$circ_{DS} \cdot [OP_D]$	[4]
Surface-Deep POP transport	73	POP_{SDP}	$5.032x10^{12}$	$kPOP_{SDP} \cdot (\frac{PP_S + xp_{SDP}}{RedCP})$	[4]
Deep POP burial	74	$POPburd_{DP}$	$4x10^9$	$kPOPbur_{DP} \cdot \left(\frac{xp_{SDP}}{CP_{oxic}}\right) \cdot (0.75 + (0.25 * [\boldsymbol{O_{DP}}]))$	[3]

OC-Organic Carbon, SRP-Soluble Reactive Phosphorous, POP-Particulate Organic Phosphorus

*Flux equation is the same as citation, however present day value is altered.

[1] – Slomp and Van Cappellen (2007)

[2] – Bergman et al. (2004)

[3] – Tsandev and Slomp (2009)

[4] – Added in this Work

Table S3: Present day parameters and constants.

Parameter/ Constant	Constant	Value	Reference
Coastal Upwelling	$kDpD$	$2.908x10^{-4}$	Slomp and Van Cappellen, 2007
Open Ocean Upwelling	$kDpS$	0.0029	Slomp and Van Cappellen, 2007
Open Ocean Downwelling	$kSDp$	0.0834	Slomp and Van Cappellen, 2007
Proximal shelf primary production	kPP_P	$3.75x10^{11}$	Slomp and Van Cappellen, 2007
Proximal organic carbon remineralisation	$kcmin_P$	$3.277x10^{13}$	This work
Proximal organic carbon burial	$kcbur_P$	0.0579	Slomp and Van Cappellen, 2007
Distal shelf primary production	kPP_D	$5.283x10^{12}$	Slomp and Van Cappellen, 2007
Distal organic carbon burial	$kcbur_D$	0.003	Slomp and Van Cappellen, 2007
Distal organic carbon remineralisation	$kcmin_D$	$5.349x10^{14}$	This work
Surface ocean primary production	kPP_S	$3.650x10^{13}$	Slomp and Van Cappellen, 2007
Surface organic carbon remineralisation	$kcmin_S$	$3.404x10^{15}$	This work
Surface to Deep Ocean export production	kxp_{SDP}	0.1265	Slomp and Van Cappellen, 2007
Deep Ocean Respiration	$kResp$	$4.921x10^{14}$	Slomp and Van Cappellen, 2007
Deep ocean organic carbon burial	$kcbur_{DP}$	0.0019	Slomp and Van Cappellen, 2007
Monod constant for respiration	kmO_2	$1x10^{-4}$	Slomp and Van Cappellen, 2007
Oxidative Weathering	$kAtmosW$	$5x10^{12}$	This work
Carbon – Phosphorus Redfield ratio	$RedCP$	106	Slomp and Van Cappellen, 2007
Oxygen - Carbon Redfield ratio	$RedOC$	106/138	Slomp and Van Cappellen, 2007

Proximal Iron bound P burial	$kFeP_P$	0.925	This work
Proximal Authigenic P burial	$kCaP_P$	$1.279x10^{-12}$	This work
Distal Iron bound P burial	$kFeP_D$	0.0014	This work
Distal Authigenic P burial	$kCaP_D$	$1.035x10^{10}$	This work
Deep ocean Iron bound P burial	$kFeP_{DP}$	$6.75x10^{9}$	This work
Deep ocean Authigenic P burial	$kCaP_{DP}$	0.0039	This work
Distal Organic P burial	$kPOPbur_D$	0.003	This work
Surface to Deep Organic Phosphorus Export Production	$kPOP_{SDP}$	0.1369	This work
Deep Ocean Organic P burial	$kPOPbur_{DP}$	0.002	This work

Supplementary Text

1. Steady-state model outputs with respect varying P input

In the main text we explore the model response to varying net surface redox by inputting reductant. The flux of reductant from the mantle has varied substantially over Earth history and undoubtedly plays some role in oxygenating the Earth, however it is also important to test our model response to different mechanisms of long-term oxygenation, specifically a long-term gradual increase in phosphorus input to the ocean. Model steady-state responses to varying riverine P input display the same overall pattern to those shown in the manuscript figure 3 (in which reductant input is varied). Increasing P input results in oxygenation of the atmosphere, followed by oxygenation events on the shelves, and finally in the deep ocean. The key difference between this plot and that shown in the manuscript is the slightly oxygenated shelf environments prior to the "GOE". This situation is created because very low P availability limits O_2 consumption in these areas. We think it is likely that both P input and changes to reductant input drove Earth's O_2 evolution, so such low values for P availability are probably unrealistic (indeed, substantial rates of silicate weathering may be required to balance the early Earth's carbon cycle under high mantle degassing rates (46)).

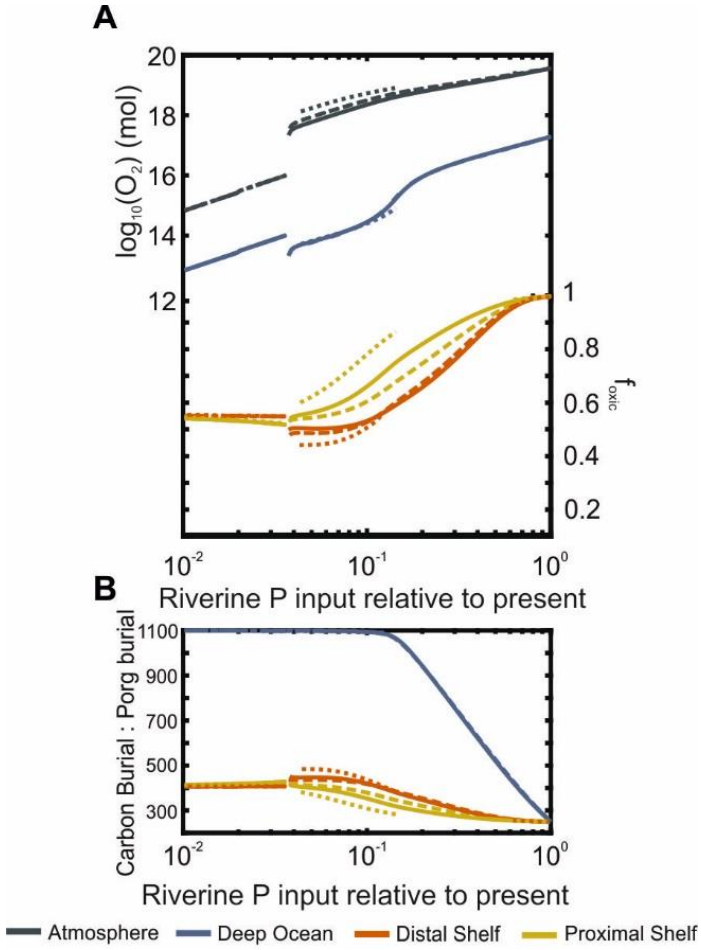

Figure S1. Steady state responses with varying riverine P input relative to present. *The f_{oxic} parameter is used to quantify the percentage of anoxic sea floor and is quantified by 1- f_{anoxic}, as described in the model (f_{anoxic} = 0.0025 present day; Watson et al., 2017). Varying redox dependencies on P_{org} and P_{auth} burial are shown for values used in previous models of Slomp and Van Cappellen, 2007 (10% - P_{auth} and 10% - P_{org}) (solid line). Greater redox dependencies are also tested (25% - P_{auth} and 50% - P_{org}, dashed line; 90% - P_{auth} and 50% - P_{org}, dotted line). Regions in which lines do not continue indicate unstable model outputs.*

2. Phosphorus scavenging in iron-rich oceans

The model on which we base our analysis was originally designed for Phanerozoic time. While the model considers ocean anoxia and its effects on the cycling of phosphorus, it does not consider the additional controls on P cycling in a ferruginous ocean (i.e. anoxic, low-sulphate and iron-rich). Under these conditions, which likely persisted for large parts of the Precambrian, it has been proposed that P would be effectively scavenged and removed from the ocean via formation of both ferrous and ferric iron compounds (e.g. Reinhard et al. 2017). Quantifying these mechanisms over deep time is an outstanding puzzle, and models are currently very poorly-constrained. But it is important to test whether the current formulation of P scavenging would effect the conclusions of this work.

In order to test the robustness of our model results we included the scavenging function used in the modelling study of Reinhard et al., (2017). As in their model, we quantify the scavenging flux by allowing a fraction of open ocean upwelled P to be buried immediately in the deep ocean sediments when deep ocean oxygen concentration is below 1μM. This results in an extremely powerful flux which can quickly deplete all ocean P, and we test various upper limits on the P burial via this mechanism. Broadly, consideration of P scavenging in an iron rich ocean does not alter the conclusions of our study. Addition of the scavenging flux alters the timings of the oxygenation events in the model by changing the relationship between overall surface redox and P cycling, but does not act to remove any of the positive feedbacks that cause the oxygenation transitions in our model. Indeed, the proposed shut-down of scavenging adds further positive feedback to the model and widens the parameter space for oscillating solutions.

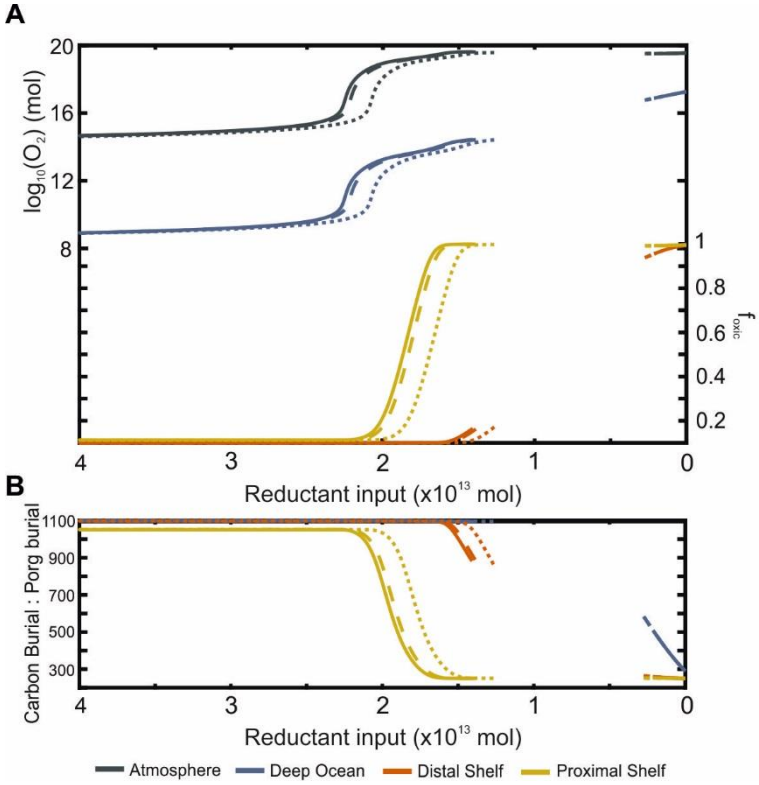

Figure S2. Steady state responses with varying reduced gas concentrations with the inclusion of the scavenging flux. *(A) The f_{oxic} parameter is used to quantify the percentage of anoxic sea floor and is quantified by 1- f_{anoxic}, as described in the model (f_{anoxic} = 0.0025 present day; Watson et al., 2017). Redox dependencies are set to values from Slomp and Van Cappellen (2007), where 50% of P_{auth} and 25% of P_{org} are redox dependent. (B) Carbon and phosphorus burial ratio in sediments. Breaks in solid lines indicate periods where no stable solution exists, in these parameter spaces the model produces an oscillating solution. (No scavenging, solid line; maximum value of 1 x 10^9 mol P/yr, dashed line; maximum value of 5 x 10^9mol P/yr, dotted line).*

3. Transient model run with estimated values of reductant.

An estimated flux of reductant into the model atmosphere over time is required to produce Figure 5. We estimate the initial flux at 4 Ga from Hayes and Waldbauer (2006) and Krissansen-Totten et al. (2018). We test both a linear and exponential decrease in the model. The linear decrease corresponds better to continental growth and change in subaerial/submarine degassing, while the exponential decrease corresponds better to mantle cooling and direct injection. This flux is highly uncertain and curves between the two shown could be used to produce very realistic timings of oxygenation in Figure 5, but we aim to avoid over-fitting and simply show results under one or other of these curves in the ms as a demonstration of Earth's oxygenation history.

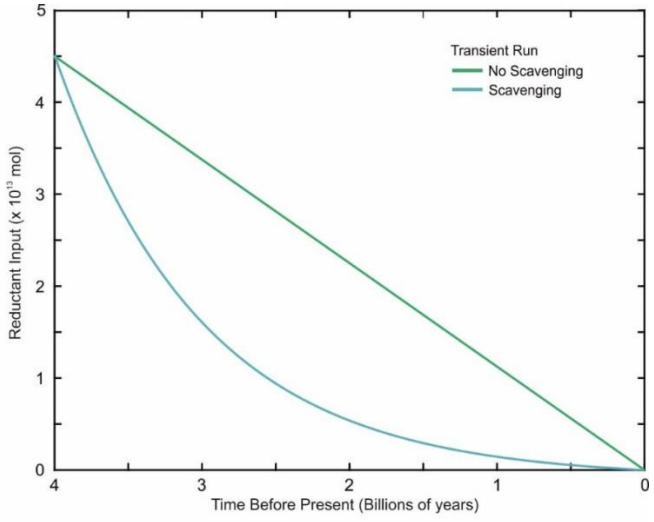

Figure S3. Estimated flux of O_2 consumption via reductant input. *Green line follows the linear decreasing trend through time, used for the transient run that did not included scavenging in Figure 5. Blue line follows an approximately exponential decrease used for the transient run that did included scavenging in Figure 5.*

4. Reactive phosphorus abundance, primary productivity and carbon burial for different model scenarios.

Figure S4 shows the SRP abundance, organic carbon burial and primary productivity for the three model scenarios explored in this work (#1: reductant-driven no scavenging (A-C), #2: reductant-driven with scavenging (D-F) and #3: phosphorus input driven (G-I)). Each model scenario has already been shown to be consistent with stepwise oxygenation, but each shows a distinctly different pattern in phosphate abundance, productivity and carbon burial. In #1, riverine P input is fixed, and P concentration is controlled solely by sedimentary burial and recycling. As recycling is more prominent under low O_2, the P concentration, productivity and burial all decrease as the reductant input declines and O_2 rises. In #2, the addition of the Fe-scavenging flux under an anoxic deep ocean results in the removal of significant amounts of SRP when the deep ocean becomes anoxic. In this scenario the SRP concentration, productivity and burial all increase as the deep ocean becomes oxygenated. Finally, in #3, reductant input is fixed and the riverine P input is varied. SRP is now controlled both by riverine input rates and recycling rates, with the former dominating the latter. Here, SRP abundance, and productivity and carbon burial all increase as P input increases.

Overall, we show here that stepwise oxygenation can occur in this model under either an increasing, static, or decreasing P inventory and C burial over Earth history.

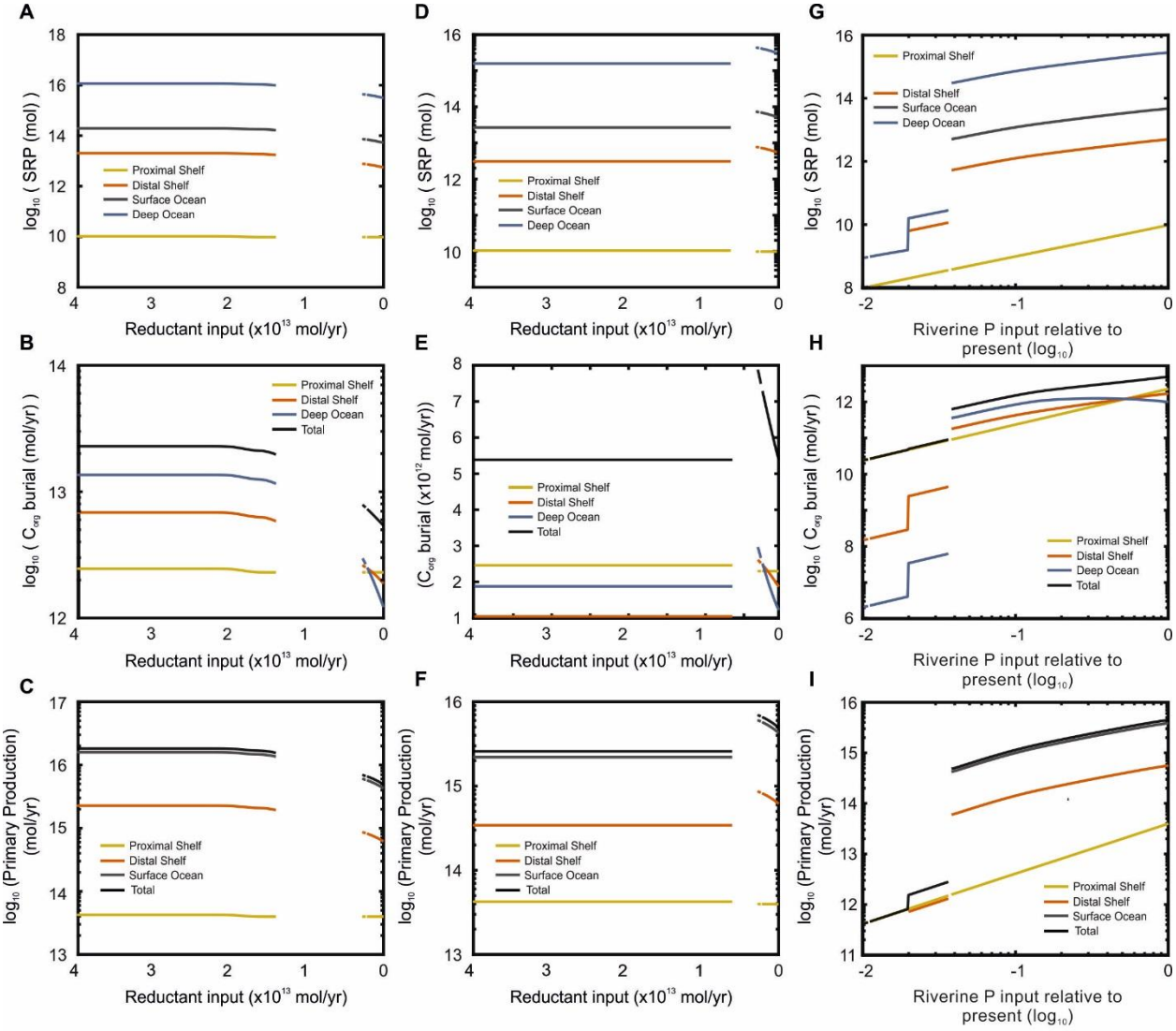

Figure S4. (A, D, G) Soluble Reactive Phosphorus (mol) for all ocean reservoirs. (B, E, H) Total C_{org} burial for all ocean-sediment fluxes (molyr^{-1}). (C, F, I) Primary production flux of organic carbon for respective ocean reservoirs (molyr^{-1}). Panels A, B and C show results in accordance with Figure 3, panels D, E and F show results in accordance with Figure S2 (scavenging included) G, H and I show results with varying riverine P input. (A, B, C) No iron-bound scavenging was used and redox dependencies of 50% - P_{auth}, 25% - P_{org} following Slomp and Van Cappellen (2007). (D, E, F) Iron bound scavenging of 25% of upwelled P (maximum value of 5 x 10^{10}) with redox dependencies following Slomp and Van Cappellen (2007) (50% - P_{auth} and 25% - P_{org}). (G, H, I) Steady state responses with varying riverine P input relative to present with redox dependencies following Slomp

and Van Cappellen (2007) (50% - P_{auth} and 25% - P_{org}). Regions where the lines do not continue represent unstable solutions.